

# Preliminary analysis of environment dimensionality by using quick 3D visualization of magnetotelluric invariants

VO Nguyen Nhu Lieu<sup>1,2</sup>, NGUYEN Van Thuan<sup>1,2\*</sup>

<sup>1</sup> University of Science, Ho Chi Minh City, Vietnam, 227 Nguyen Van Cu Street, District 5, Ho Chi Minh City, Vietnam

<sup>2</sup> Vietnam National University, Ho Chi Minh City, Vietnam, Linh Trung Ward, Thu Duc City, Ho Chi Minh City, Vietnam.

\* Corresponding email: [nvthuan@hcmus.edu.vn](mailto:nvthuan@hcmus.edu.vn)

**Abstract:** Magnetotelluric method could express Earth structures through images of electrically resistivity distribution in 1D, 2D and 3D views. Although it is affected by non-unique of solutions, it is one of the great methods to investigate the Earth in the big depth. Magnetotelluric inversion is one effecting way to recover resistivity information of the measured area. However, it is time consuming in computing and labour resource efforts. We would like to suggest on workflow in which we can interpret the magnetotelluric data quickly and efficiently. Normally, raw data is hardly interpreted but existence of the Earth parameter as resistivity could relate to invariants of magnetotelluric data. We suggest Zs-Zp invariants to image the Earth briefly by taking use of their Zs-Zp structural images. We apply the workflow into 3D modelling data and real data measured in Australia. We compare the Zs-Zp invariants structures with the correct boundary information of the 3D model. For the real data, we use seismic data and seismic attributes to have correct boundary and geology structures to valid the correction of the Zs-Zp with the seismic information.

**Keywords:** Magnetotelluric; Invariant; Zs-Zp

## 1. Introduction

The magnetotelluric (MT) approach, a powerful geophysical exploration technique, is used to investigate the Earth's subsurface electrical conductivity. It relies on natural variations in the Earth's magnetic and electric fields to map conductivity structures at various depths. These natural variations are caused by geomagnetic pulsations and interactions between solar wind and the Earth's magnetosphere (Berdichevsky & Dmitriev, 2008, Siniscalchi et al., 2020).

Since its inception in the mid-20th century, the MT method has been extensively applied in mineral exploration, hydrocarbon detection, geothermal energy mapping, and tectonic studies (Berdichevsky & Dmitriev, 2008, Siniscalchi et al., 2020). By analyzing the electromagnetic field relationship between the measured electric and magnetic fields, geophysicists can infer subsurface properties and identify geological structures, such as mineral deposits, fault zones, and aquifers. The non-invasive nature of method and ability to probe deep geological layers make it an invaluable tool for understanding the Earth's interior.

The survey depth in magnetotelluric (MT) studies is primarily determined by the electromagnetic wave frequency. The relationship is given by the skin depth formula (1) (Berdichevsky & Dmitriev, 2008, Naidu, 2012):

$$p(T) \approx 500\sqrt{T\rho_a} \quad (1)$$

Where:  $\rho_a$  - apparent resistivity; T - wave period and p(T) - penetration depth corresponding wave period. This formula indicates that lower frequencies can penetrate deeper into the Earth, allowing for the investigation of deeper subsurface structures. Whereas higher frequencies provide information about shallower depths.

Based on the formula (1), and assuming the medium resistivity of the Earth's crust and the upper part of the mantle as 100  $\Omega\text{m}$ , it can be seen that the wave propagation depth is from 160 m to more than 500 km (these depths may reach the upper layer of the mantle). The very large survey depth is the outstanding advantage of MT compared to other artificial geoelectric methods.

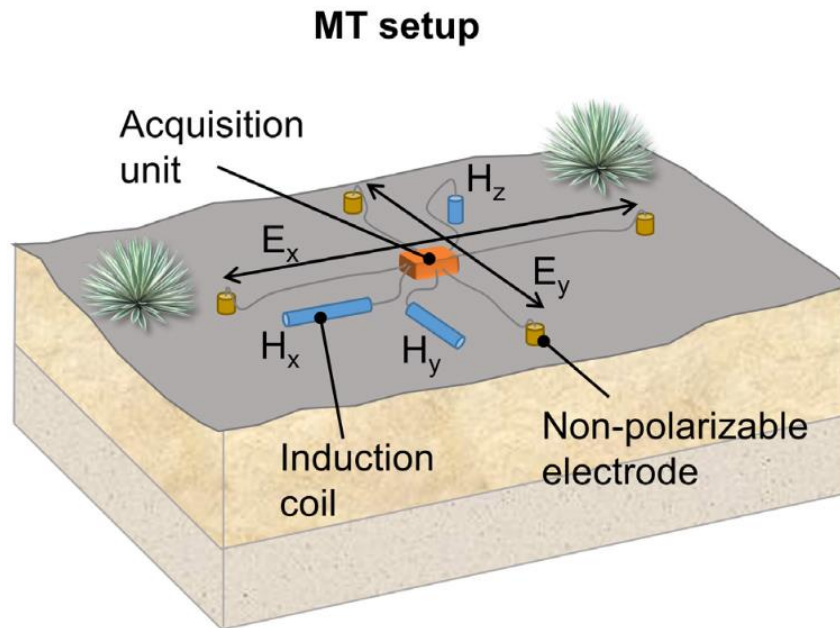


**Fig. 1.** Measuring equipment arrangement in magnetotelluric (Bücker et al., 2017)

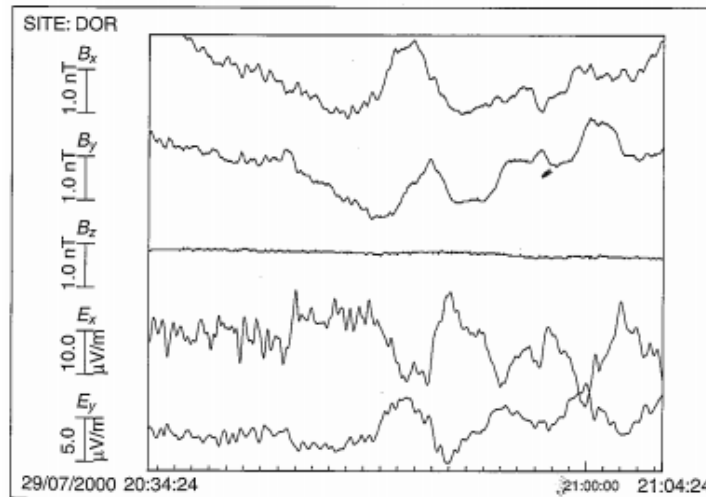


**Fig. 2.** Five components, two of electric field:  $E_x$  and  $E_y$ , and three of magnetic field:  $B_x$ ,  $B_y$  and  $B_z$  obtained after the measurement (Simpson & Bahr, 2005)

The relationship between the electric field and the magnetic field is represented through impedance tensor  $Z$  (2) (Eggers, 1982, Berdichevsky & Dmitriev, 2008, Naidu, 2012)

$$\hat{Z} = \begin{pmatrix} Z_{xx} & Z_{xy} \\ Z_{yx} & Z_{yy} \end{pmatrix} \quad (2)$$

The impedance tensor plays a decisive role, representing the linear relationship of the electromagnetic field and the Earth's conductive structure. Therefore, researching and extracting useful scalar parameters from this tensor is of great interest, leading to many methods of developing it.

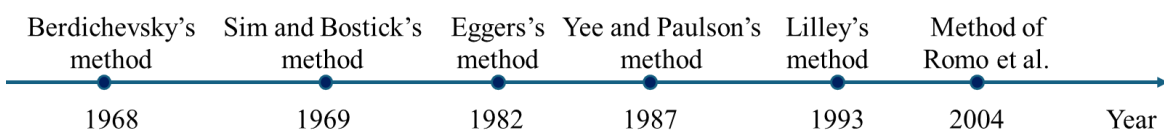


**Fig. 3.** Tensor analysis methods over the years (Berdichevsky, 1968, Sims & Bostick Jr, 1969, Eggers, 1982, Yee & Paulson, 1987, Lilley, 1993, Romo et al., 2004)

Invariants are derived from the magnetotelluric impedance tensor, which is a complex matrix representing the relationship between the electric and magnetic fields (Berdichevsky, 1968, Sims & Bostick Jr, 1969, Eggers, 1982, Yee & Paulson, 1987, Lilley, 1993, Romo et al., 2004). The invariants are quantities that remain unchanged under rotation of the coordinate system. The impedance tensor has both real ( $ReZ$ )

and imaginary (ImZ) parts, and the invariants are calculated from these components. Common invariants include the real and imaginary components of the determinant of the impedance tensor, as well as the trace and the sum of squares of the elements (Berdichevsky, 1968, Sims & Bostick Jr, 1969, Eggers, 1982, Yee & Paulson, 1987, Lilley, 1993, Romo et al., 2004).

Using invariants helps to simplify the MT data interpretation by reducing the complexity of the data analysis. Since invariants are independent of the coordinate system, they provide a more robust and reliable way to interpret subsurface conductivity structures. Invariants are used to map subsurface conductivity, identify geological structures, and explore mineral resources (Berdichevsky, 1968, Sims & Bostick Jr, 1969, Eggers, 1982, Yee & Paulson, 1987, Lilley, 1993, Romo et al., 2004). They are particularly useful in areas with complex geology, where traditional methods might struggle to provide clear results.

## 2. Methodology

### 2.1. Overview of MT data

Apparent resistivity is a measure of the subsurface resistance to the flow of electrical current, as inferred from surface measurements of electric and magnetic fields. It is a function of frequency and provides insights into the distribution of electrical conductivity at different depths (Berdichevsky & Dmitriev, 2008, Siniscalchi et al., 2020).

The apparent resistivity ( $\rho_a$ ) is derived from the impedance tensor ( $Z$ ) and is specifically calculated from the magnitude of the impedance tensor components (Berdichevsky & Dmitriev, 2008, Siniscalchi et al., 2020). The relationship can be expressed as (3):

$$\rho_{a,ij} = \frac{\mu_0}{2\pi f} |Z_{ij}|^2 \tag{3}$$

where:  $f$  - frequency,  $\mu_0$  - magnetic constant.

### 2.2. Invariants computing from Zs-Zp method

The  $Z_S$ - $Z_P$  invariants in magnetotelluric (MT) studies are rotational invariants of the impedance tensor (Romo et al., 2004). These invariants are crucial because they provide a way to analyse the data without being affected by the orientation of the measurement system.

- Series Impedance ( $Z_S$ ): This is more sensitive to galvanic effects and represents the current flow across interfaces.
- Parallel Impedance ( $Z_P$ ): This is more sensitive to inductive effects and represents the current flow along interfaces.

We assume that the total impedance of the electromagnetic field observed in the x-y coordinate system is transformed to the new x'-y' coordinate system by applying a rotation matrix  $R$ . The electric field rotates the angle  $\theta_e$  (applying rotation matrix  $R_e$ ), the magnetic field rotates the angle  $\theta_h$  (applying rotation matrix  $R_h$ ) (Romo et al., 2004).

$$R_e E = R_e Z H = R_e Z R_h^T R_h H = Z' R_h H \tag{4}$$

where:  $Z' = \begin{pmatrix} 0 & Z_1 \\ Z_2 & 0 \end{pmatrix}$  - the transformed impedance;  $R_c = \begin{pmatrix} \cos \theta_c & \sin \theta_c \\ -\sin \theta_c & \cos \theta_c \end{pmatrix}$  - the rotation matrix and symbol c stands for e or h; and  $R_c^T$  - stands for the transposed rotation matrix for either c.

From many transformations, the total impedance tensor in the x-y axis system can be equivalently expressed in the following form (5) (Romo et al., 2004):

$$\{Z_{xx}, Z_{xy}, Z_{yx}, Z_{yy}\} \Leftrightarrow \{Z_1, Z_2, \theta_e, \theta_h\} \Leftrightarrow \{Z_S, Z_P, \bar{\theta}, \Delta\theta\} \tag{5}$$

$$\text{where: } Z_1 = \frac{1}{2} \left[ \frac{(Z_{xy} + Z_{yx})}{\cos(\theta_e + \theta_h)} + \frac{(Z_{xy} - Z_{yx})}{\cos(\theta_e - \theta_h)} \right] \text{ and } Z_2 = \frac{1}{2} \left[ \frac{(Z_{xy} + Z_{yx})}{\cos(\theta_e + \theta_h)} - \frac{(Z_{xy} - Z_{yx})}{\cos(\theta_e - \theta_h)} \right]; \bar{\theta} = \frac{\theta_e + \theta_h}{2}$$

- the arithmetic average;  $\Delta\theta = \theta_e - \theta_h$  - the angular difference;  $Z_S$  - Series Impedance and  $Z_P$  - Parallel Impedance.

In the 2D case,  $Z_S$  and  $Z_P$  can be written (Romo et al., 2004):

$$Z_s = \frac{Z_1 + Z_2}{2 \sin \varphi} \tag{6}$$

$$Z_p = \frac{2Z_1Z_2 \sin \varphi}{Z_1 + Z_2} \tag{7}$$

where:  $\varphi = a \tan \left( \frac{Z_2 + Z_1}{Z_2 - Z_1} \right)$

The existence of an inverse transformation confirms that information will not be lost if we use  $\{Z_s, Z_p, \bar{\theta}, \Delta\theta\}$  instead of the original value  $\{Z_{xx}, Z_{xy}, Z_{yx}, Z_{yy}\}$  (Romo et al., 2004).

By analyzing these invariants, geophysicists can better understand the subsurface conductivity and identify geological structures. Substituting impedances ( $Z_{xx}, Z_{xy}, Z_{yx}, Z_{yy}, Z_s$  and  $Z_p$ ) in Eq. (5) into Eq. (3), the components of resistivities ( $R_{xx}, R_{xy}, R_{yx}, R_{yy}, \rho_{zs}$  and  $\rho_{zp}$ ) are defined, respectively.

### 3. Results

#### 3.1. Modelling

The modelling data is computed from the oblique conductor model. We used “Oblique Conductor model” because the angle between the 3D block’s major axis and the direction of the boundary of the two 2D resistive structures is  $45^\circ$  (Ledo, 2005). In the 3D model extracted from the works (Tietze & Ritter, 2013, Tietze et al., 2015) (Fig. 4), a regional 2-D resistivity block exists within two half-layers of  $50 \Omega\text{m}$  and  $500 \Omega\text{m}$  between 0.1 km and 70.8 km depth; the top ( $<0.1$  km) and bottom ( $>75$  km) layers are set to  $100 \Omega\text{m}$  (Ledo, 2005). In the center zone, the 3D most conductive  $5 \Omega\text{m}$  block of  $30 \text{ km} \times 9 \text{ km} \times 9 \text{ km}$  (length  $\times$  width  $\times$  height) lies with its top interface at the depth 2.56 km. The angle between the 3D one’s the major axis and the direction of the boundary of the two 2D resistive structures is  $45^\circ$  (Fig. 4).

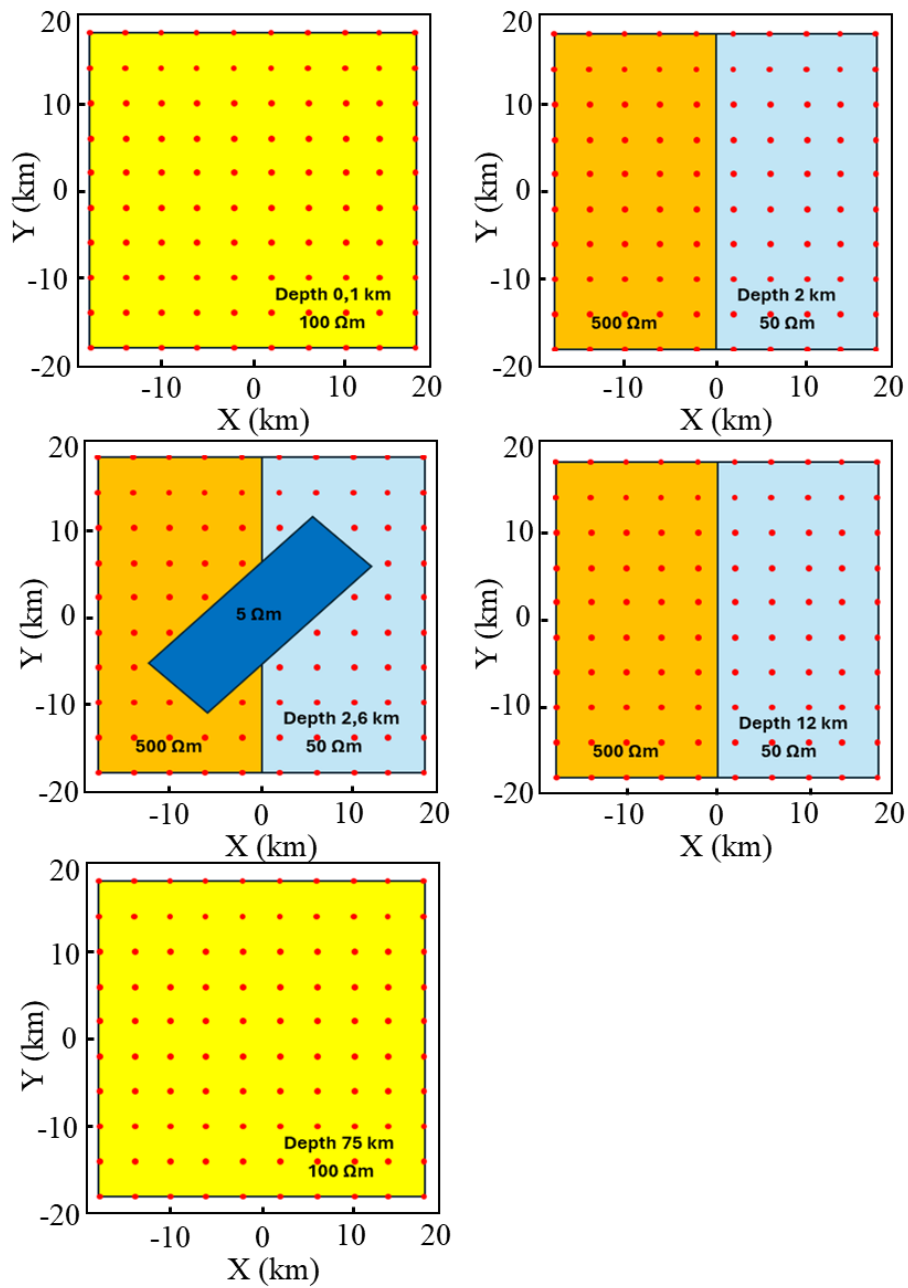


**Fig. 4.** 3D model extracted from the works (Tietze & Ritter, 2013, Tietze et al., 2015)

We have calculated distribution of resistivity of series and parallel impedance in the three dimensional  $-x, y$ , period (Fig. 5) described in Sect.2 (using Eq. (6) and (7)). Series impedance represents the conductive block in the centre domain better than parallel impedance. Moreover, it also represents clearly the boundary between the two blocks  $50 \Omega\text{m}$  and  $500 \Omega\text{m}$ .

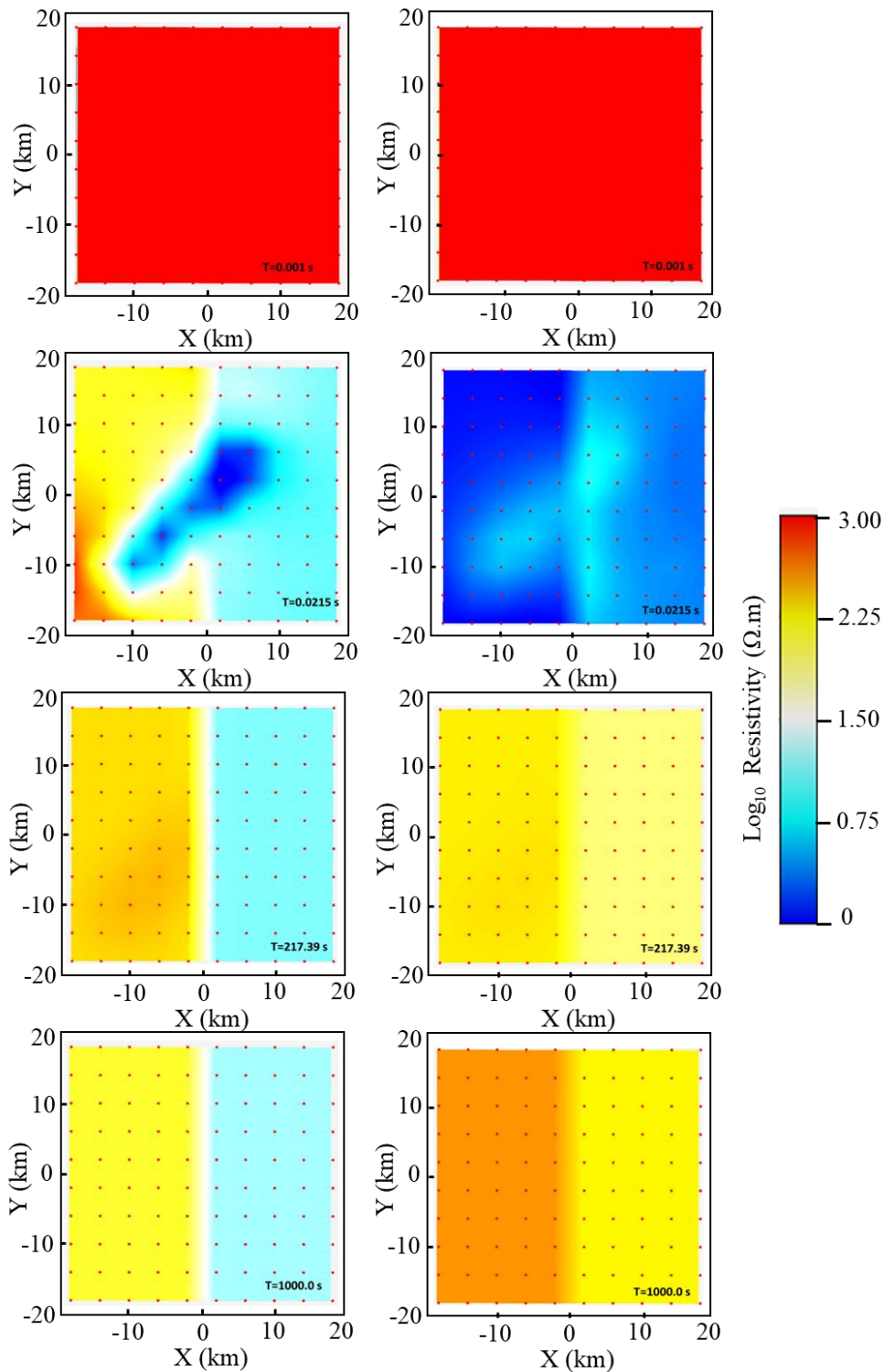


**Fig. 5.** RhoZs (left column) and RhoZp (right column) sections according to periods: T=0.001 s, T=0.0215 s, T=217.39 s, T=1000 s

For comparing the resistivity with real model, we design three slices of the resistivity (Fig. 6). For  $z_1$  plane (period plane), the most conductive object in the model is seen in the most conductive zone of the resistivity of series impedance. Moreover, the difference of the two zones as medium conductive and most resistive in model is also visualized in the plane. The values of the resistivity of Zs are 374  $\Omega\text{m}$  and 50  $\Omega\text{m}$ , respectively, are reasonable to the real value of the model. For  $y_1$  plane, again, two zones of the real model can be separated.

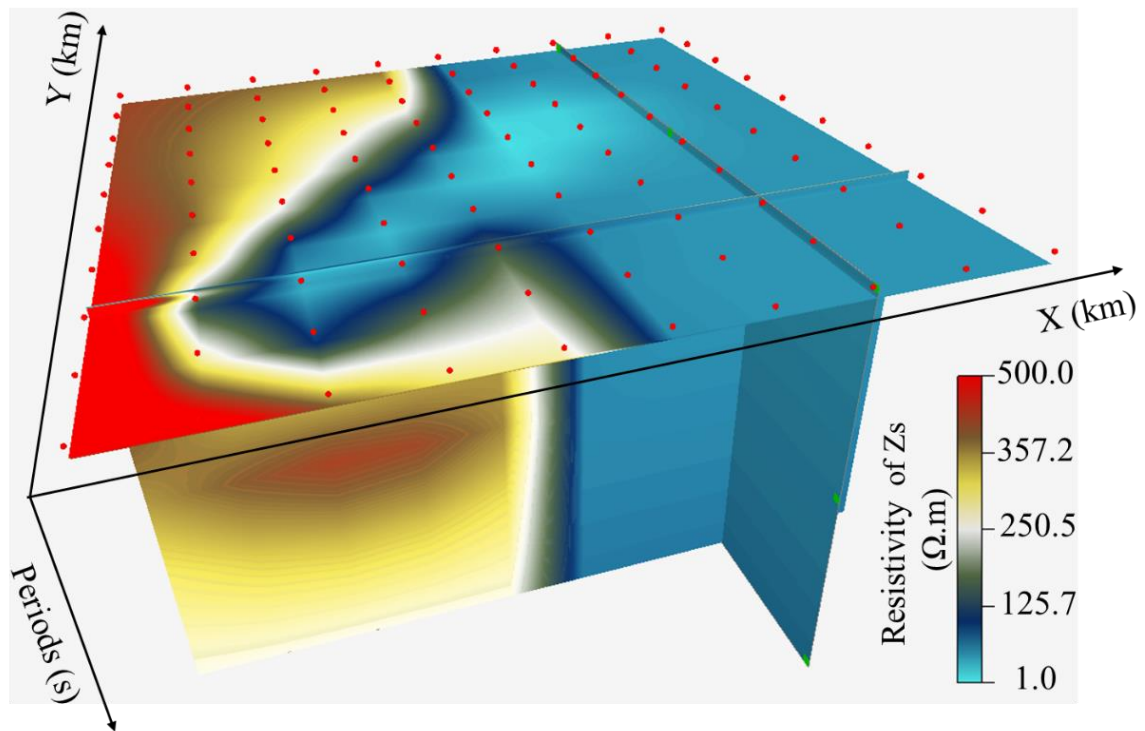


**Fig. 6.** Representation of resistivity of series impedance,  $Z_s$ . There are three slices in  $z_1$  plane (period plane),  $y_1$  plane and  $x_1$  plane to show the most conductive, medium conductive and the least conductive, respectively.

**3.2. Real data in Olympic Dam area, Australia**

We use data measured in the Olympic Dam area, southern Australia. This data is published by Geoscience Australia (Australia, 2025). The locations of the 81 MT stations and the seismic lines are illustrated in Fig. 7. We use  $Z_s$ - $Z_p$  method to process 81 MT sites and match them with the seismic data as Fig. 7.

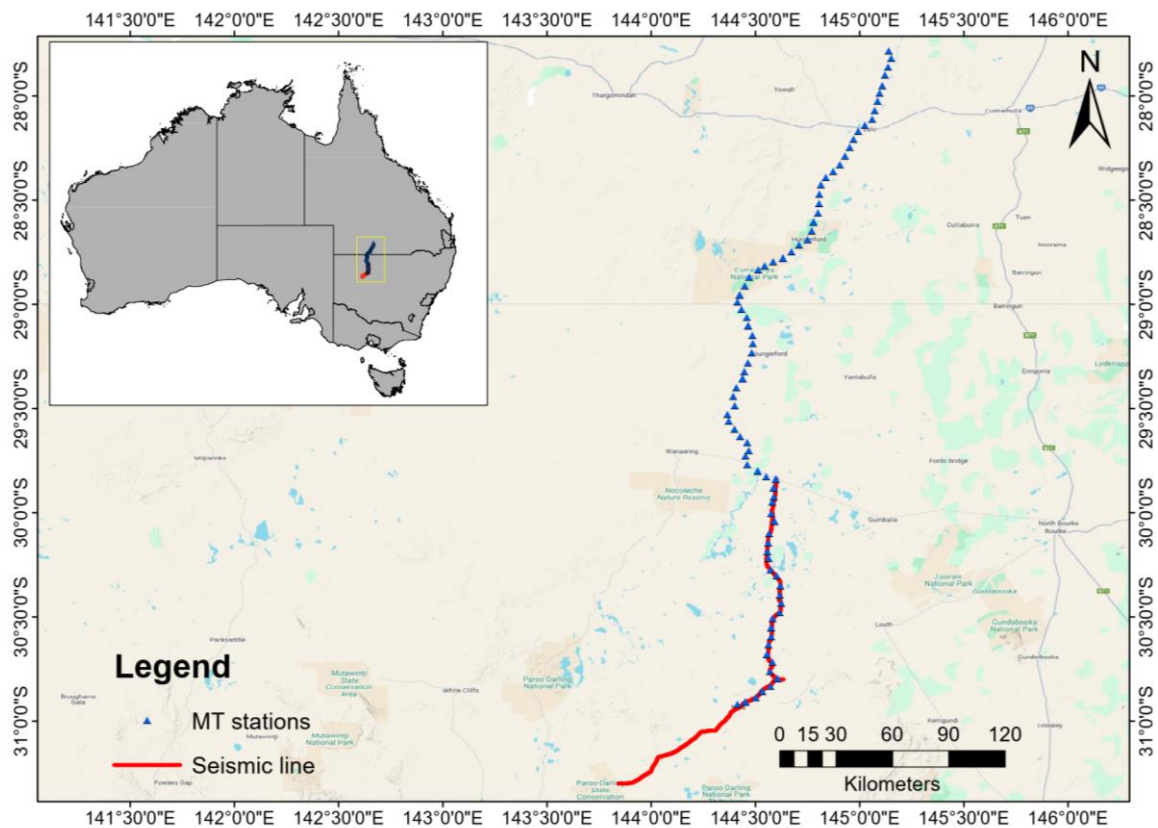


**Fig. 7.** Magnetotelluric (the symbol of triangle) and seismic survey (the red line) area (modified from the data at (Australia, 2025))

We have calculated distribution of resistivity of series and parallel impedance in the two dimensional space:  $x$  vs. period. In Fig. 8, we present resistivity sections  $R_{xx}$ ,  $R_{xy}$ ,  $R_{yx}$ ,  $R_{yy}$ ,  $RhoZ_s$ ,  $RhoZ_p$  and the known seismic plane, respectively. The length of the seismic measurement line (the red line) is shorter than the MT line (the symbol of triangle) ( Fig. 7).

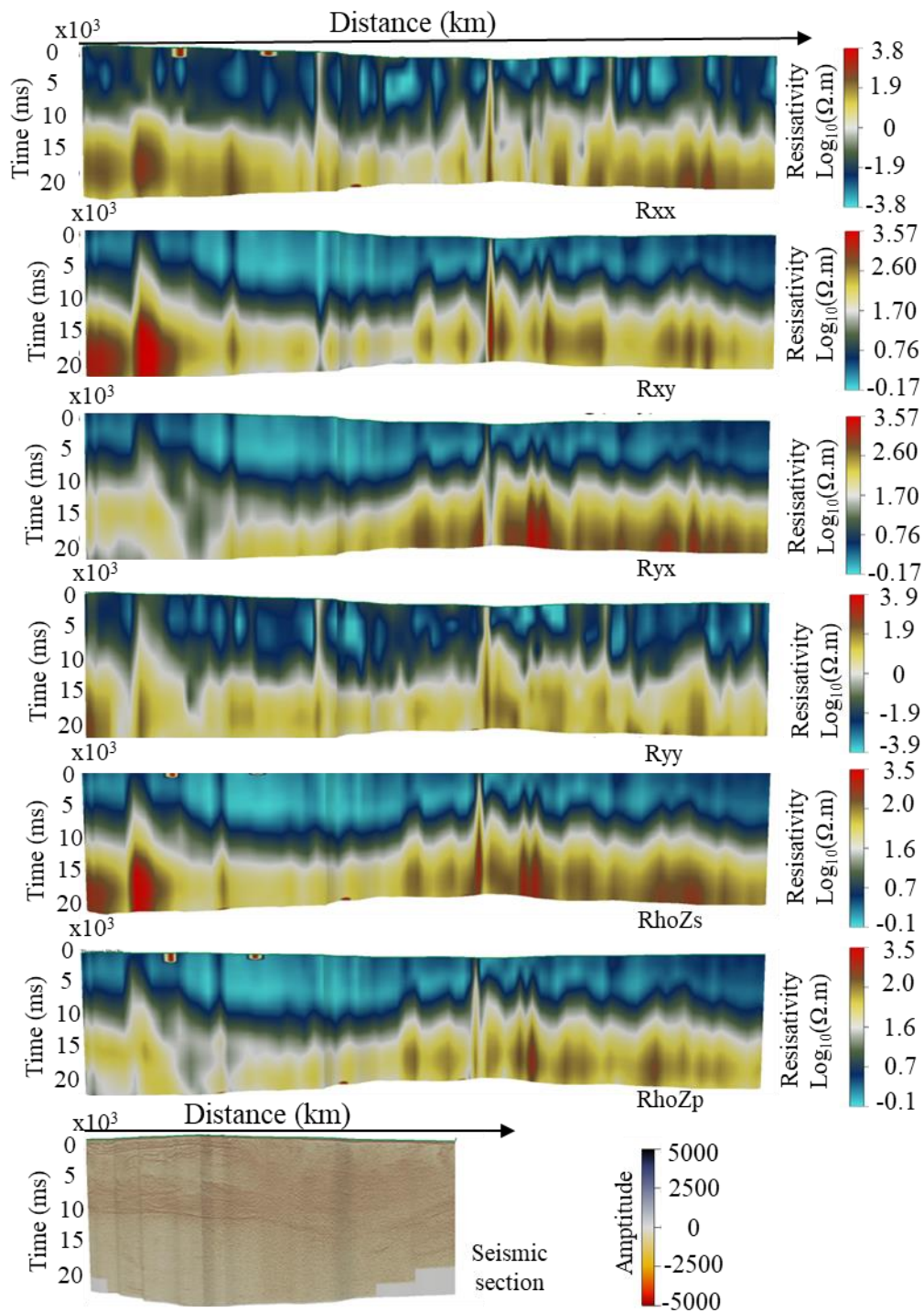


**Fig. 8.** Resistivity sections from 84 MT sites and image of seismic

We present images of seismic amplitude, resistivity of  $Z_s$  and the boundaries between layers with different resistivities (see Fig. 9). The seismic raw data is of high quality for interpretation. Resistivity of  $Z_s$  can show different zones of resistivity values as conductive and resistive according to depths.

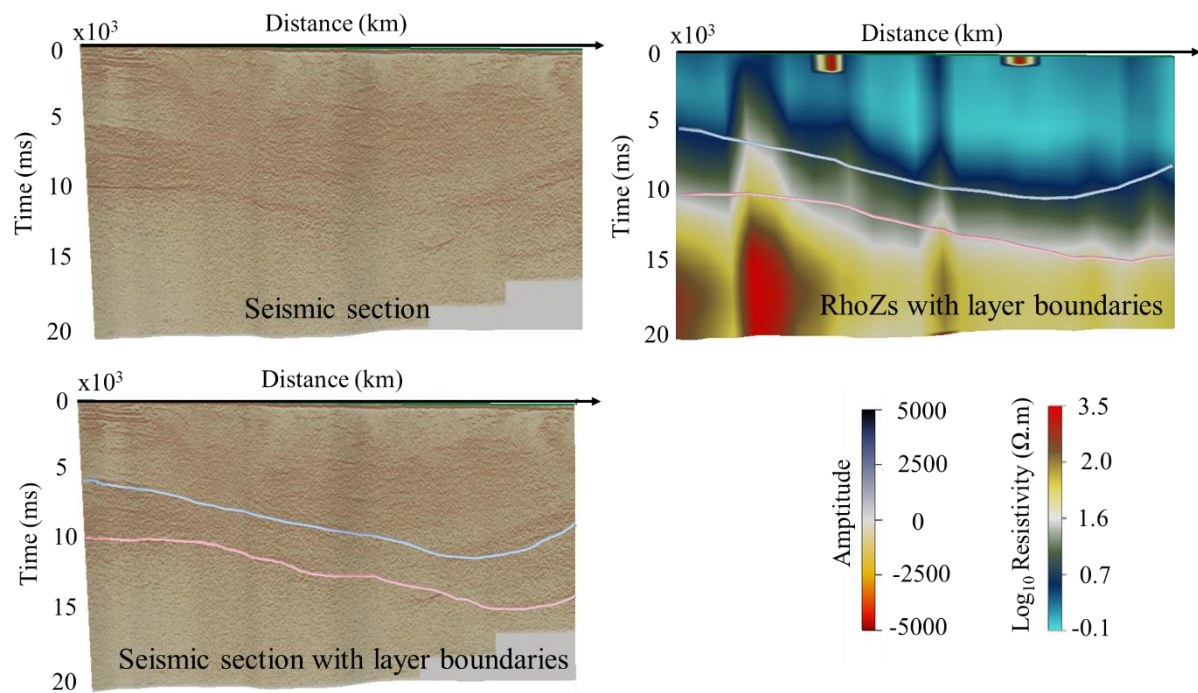


**Fig. 9.** Similarity of layer boundaries in MT method and seismic method.

#### 4. Conclusion

Through 3D modeling and field data results, we find that the Zs-Zp method gives quite good conclusions in representing the heterostructure and the boundaries of the resistivity layers. By using the invariants Zs - Zp we can quickly image the structure of the Earth.

#### Acknowledgements

This research is funded by Vietnam National University, Ho Chi Minh City (VNU-HCM) under grant number C2023-18-07. We would thank Geoscience Australia, Australian Government for providing access to geophysical data. We also thank to dGB Earth Sciences and Curtin University for providing access to software tools. Lastly, we deeply appreciate our mentor, Associate Professor Cuong Van Anh Le, Head of Department of Geophysics, Faculty of Physics and Engineering Physics (VNU-HCM), for his assistance and guidance. Authors thank the anonymous reviewers to help in improvement the paper.

#### Conflicts of Interest

The authors declare no conflict of interest.

#### Author Contribution

All the authors contribute to analysis and interpretation of geophysical data and manuscript writing.

#### Literature – References

1. Australia G, 2025. Geoscience Australia Portal. In.: Geoscience Australia.
2. Berdichevsky MN, 1968. Electrical prospecting by the method of Magnetotelluric Profiling. *Nedra, Moscow* **140**, 153.
3. Berdichevsky MN, Dmitriev VI, 2008. *Models and methods of magnetotellurics*. Springer Science & Business Media.
4. Bücke M, Lozano García S, Ortega Guerrero B, *et al.*, 2017. Geoelectrical and electromagnetic methods applied to paleolimnological studies: Two examples from desiccated lakes in the Basin of Mexico. *Boletín de la Sociedad Geológica Mexicana* **69**, 279-98.
5. Eggers DE, 1982. An eigenstate formulation of the magnetotelluric impedance tensor. *J Geophysics* **47**, 1204-14.
6. Ledo J, 2005. 2-D versus 3-D magnetotelluric data interpretation. *Surveys in Geophysics* **26**, 511-43.
7. Lilley F, 1993. Magnetotelluric analysis using Mohr circles. *Geophysics* **58**, 1498-506.
8. Naidu GD, 2012. Magnetotellurics: Basic theoretical concepts. *Deep Crustal Structure of the Son-Narmada-Tapti Lineament, Central India*, 13-35.

9. Romo JM, Gómez-Treviño E, Esparza FJ, 2004. Series and parallel transformations of the magnetotelluric impedance tensor: theory and applications. *Physics of the earth planetary interiors* **150**, 63-83.
10. Simpson F, Bahr K, 2005. *Practical magnetotellurics*. Cambridge University Press.
11. Sims WE, Bostick Jr FX, 1969. Methods of magnetotelluric analysis: Tech. Rep. 58, Electr. *Geophys. Res. Lab., Univ. Of Texas at Austin*.
12. Siniscalchi A, Romano G, Tripaldi S, 2020. Magnetotellurics: An Overview. *Encyclopedia of Geology, 2nd edition* **1**, 698-705.
13. Tietze K, Ritter O, 2013. 3D magnetotelluric inversion in practice - the electrical conductivity structure of the San Andreas Fault in Central California. *Geophysical Journal International* **195**, 130-47.
14. Tietze K, Ritter O, Egbert GD, 2015. 3-D joint inversion of the magnetotelluric phase tensor and vertical magnetic transfer functions. *Geophysical Journal International* **203**, 1128-48.
15. Yee E, Paulson K, 1987. The canonical decomposition and its relationship to other forms of magnetotelluric impedance tensor analysis. *J Journal of Geophysics* **61**, 173-89.